Collisionless shock acceleration of narrow energy spread ion beams from mixed species plasmas using 1 μm lasers

A. Pak,[1,*] S. Kerr,[2] N. Lemos,[1] A. Link,[1] P. Patel,[1] F. Albert,[1] L. Divol,[1] B. B. Pollock,[1] D. Haberberger,[3] D. Froula,[3] M. Gauthier,[4] S. H. Glenzer,[4] A. Longman,[2] L. Manzoor,[2] R. Fedosejevs,[2] S. Tochitsky,[5] C. Joshi,[5] and F. Fiuza[4,†]

[1]*Lawrence Livermore National Laboratory, Livermore, California 94550, USA*
[2]*Department of Electrical and Computer Engineering, University of Alberta, Edmonton, Alberta T6G 2V4, Canada*
[3]*Laboratory for Laser Energetics, University of Rochester, 250 East River Road, Rochester, New York 14623-1299, USA*
[4]*SLAC National Accelerator Laboratory, Menlo Park, California 94025, USA*
[5]*Department of Electrical Engineering, UCLA, Los Angeles, California 90095, USA*

(Received 6 October 2017; published 25 October 2018)

Collisionless shock acceleration of protons and C^{6+} ions has been achieved by the interaction of a 10^{20} W/cm^2, 1 μm laser with a near-critical density plasma. Ablation of the initially solid density target by a secondary laser allows for systematic control of the plasma profile. This enables the production of beams with peaked spectra with energies of 10–18 MeV/amu and energy spreads of 10%–20% with up to 3×10^9 particles within these narrow spectral features. The narrow energy spread and similar velocity of ion species with different charge-to-mass ratios are consistent with acceleration by the moving potential of a shock wave. Particle-in-cell simulations show shock accelerated beams of protons and C^{6+} ions with energy distributions consistent with the experiments. Simulations further indicate the plasma profile determines the trade-off between the beam charge and energy and that with additional target optimization narrow energy spread beams exceeding 100 MeV/amu can be produced using the same laser conditions.

DOI: 10.1103/PhysRevAccelBeams.21.103401

I. INTRODUCTION

The ability to study the properties of high energy density matter in the laboratory is expanding our understanding of the physics associated with inertial fusion targets, planetary interiors, and astrophysical systems [1–3]. Laser-produced ion beams have proven an invaluable tool for both creating and probing such high energy density matter [4–8]. Traditionally, these beams have been accelerated via the target normal sheath acceleration (TNSA) mechanism, which produces a continuous exponentially decreasing energy spectrum [9]. In the pursuit of new applications and increased precision, significant effort has gone into exploring other schemes to extend the maximum ion energy and reduce the energy spread to 1%–10% [10–17]. Recently, proof-of-principle experiments have shown that such narrow energy spread proton beams, containing 2×10^5 particles, can be accelerated up to ~20 MeV in tailored near-critical density plasmas via an electrostatic shock wave driven in a hydrogen gas jet plasma by a 10 μm CO_2 laser [18,19]. While these results are promising, CO_2 lasers are not commonly available. Furthermore, it is desirable to produce beams with higher charge and particle energy, which generally requires operating at higher densities and intensities. This can be achieved only by using more ubiquitous solid-state high-intensity lasers at a wavelength of ~1 μm.

Here, we report for the first time on collisionless shock acceleration (CSA) experiments with a 1 μm laser that produced proton and ion beams with narrow energy spreads $\Delta E/E$ of 10%–20% centered at 10–18 MeV/amu and with a total number of particles in these peaks up to 3×10^9. To produce a plasma density profile suitable for CSA, we have used a secondary laser to ablate a Mylar ($C_{10}H_8O_4$) foil. For this profile, we observed similar velocity distributions of accelerated protons and heavier ions, consistent with the reflection from the moving potential of an electrostatic shock. The number of particles within the narrow distributions of accelerated ions is ~$10^4\times$ larger than obtained in previous CSA experiments [18]. Two-dimensional (2D) particle-in-cell (PIC) simulations that model the laser

*Corresponding author.
pak5@llnl.gov
†Corresponding author.
fiuza@slac.stanford.edu

interaction with a CH plasma for the experimental conditions show CSA of multiple ion species with spectra consistent with observations. An analysis of simulation results reveals that the plasma density profile determines the trade-off between the energy gain and number of accelerated particles, by controlling the velocities of the shock and of the expanding plasma. This suggests that further control over the density profile could allow beams to be tuned according to application needs.

II. COLLISIONLESS SHOCK FORMATION

The formation of a collisionless electrostatic shock requires the creation of a localized region of higher pressure within a plasma with $T_e \gg T_i$ [20–22]. The interaction of a high-intensity laser with a near-critical density plasma can efficiently produce these conditions [21]. As this region of high pressure expands, it can drive a shock wave with velocity $v_s = M_s C_s$ into the surrounding lower-pressure plasma. Here v_s is defined in the upstream plasma frame, M_s denotes the shock Mach number, and for $T_e \gg T_i$ the ion sound speed $C_s = (ZT_e/m_i)^{1/2}$ depends on the electron temperature T_e, the ion mass m_i, and the ion charge state Z of the plasma. The shock can reflect upstream ions if its electrostatic potential $Ze\Phi$ is larger than the kinetic energy of the in-flowing ions, i.e., $\bar{\Phi} = Ze\Phi/(\frac{1}{2}m_i v_s^2) > 1$. Provided this criterion is satisfied, the shock can reflect ions of different charge-to-mass (Z/m_pA) ratios to a velocity $2v_s$. The final ion velocity will result from contributions from both shock reflection and sheath acceleration (which depends on the plasma profile) and can be written as $v_f = 2v_s + v_{\text{sheath}}$.

To produce high-energy ($\gtrsim$10 MeV/amu) ion beams with moderate strength shocks ($1 < M_s < 3$), the plasma needs to be heated to $T_e \gtrsim 1$ MeV to drive a shock with $v_s \gtrsim 0.1$ c. Balancing the energy density of the laser with that of the target, T_e can be estimated as [21]

$$T_e[\text{MeV}] = 2.6\eta a_0^2 \frac{n_c}{n_e}\frac{\tau_0[\text{ps}]}{L[10\ \mu\text{m}]}, \tag{1}$$

where τ_0 is the laser pulse duration, L is the target thickness, n_e is the electron density, $n_c \approx 10^{21}$ cm^{-3} is the critical density for 1 μm light, and $a_0 = \frac{eA}{m_e c^2}$ is the normalized vector potential of the laser. At a high laser intensity ($a_0 \gg 1$), the coupling of the laser to the target, η, can be optimized to values of ~0.5 for a peak electron density near the relativistic critical density $n_e = a_0 n_c$ [23]. To explore CSA in this high-intensity regime, experiments were performed at the Titan laser facility.

III. EXPERIMENT

As seen in Fig. 1(a), to produce a near-critical density target, the 0.5-μm-thick Mylar foil was first irradiated by the 10-ns-long, 1 μm wavelength ablation laser focused to a

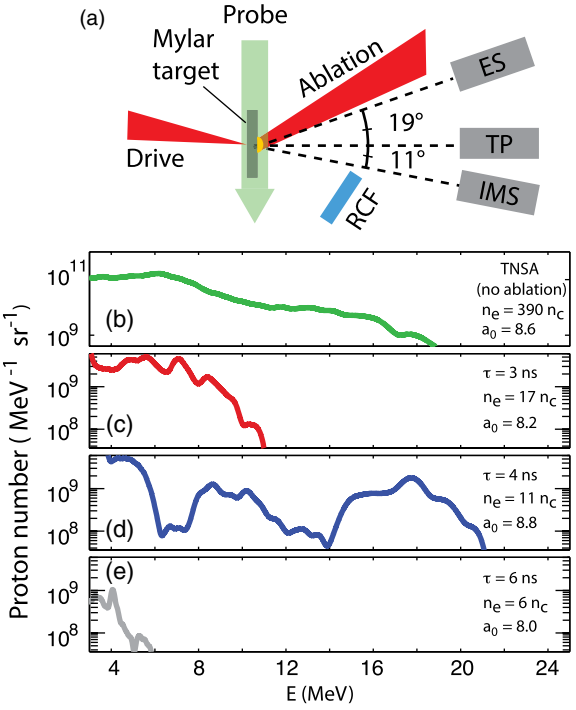

FIG. 1. (a) Experimental setup. A near-critical density target is created by first irradiating a Mylar foil with an ablation laser. After the target has expanded for a time τ, a high-intensity picosecond duration laser pulse is focused onto the target to produce the electrostatic shock wave. Accelerated ions are measured by the imaging magnetic spectrometer (IMS) and Thomson parabola (TP). TP measurements indicate the majority of accelerated ions are C^{6+}/O^{8+}. Accelerated electrons are measured by a permanent magnet electron spectrometer. Radiochromic film (RCF) was used to measure a portion of the spatial beam profile. Orthogonal to the target, a probe laser was used to measure the target expansion. Accelerated proton spectra shown (b) for an unablated foil and (c)–(e) at different time delays from consecutive shots. The inferred peak n_e of the target and laser a_0 are also denoted. Only a signal of $> 4\times$ the background variation is shown.

diameter of ~550 μm and an average peak intensity of 1.2×10^{11} W/cm^2. This approach was pursued in order to produce plasmas with peak densities of $\sim 10 n_c$ and lengths $L \leq 50$ μm required to obtain $T_e > 1$ MeV using a drive laser $a_0 \sim 10$ per Eq. (1). The ablation of material creates a density gradient and an associated quasiuniform sheath field that allows the shock-reflected ions to exit the target with their narrow energy spread largely preserved [24,25]. After the target expansion, an high-intensity drive laser, with a wavelength of 1 μm and a duration of ~1 ps, was focused onto the plasma to generate the shock wave. The longitudinal position of the target was varied by up to 150 μm. This changed the full width at half maximum (FWHM) of the laser spot from 5 to 9 μm and peak a_0 from ~4.5 to 8.5, respectively.

To optimize the CSA process, the peak plasma density and profile were changed by varying the delay τ between the beginning of the ablation laser and the high-intensity

short pulse drive laser. Shadowgraphic measurements of the foil ablation [26] were found to be consistent with radiation hydrodynamic calculations using the code HYDRA [27]. These calculations indicate that the peak density decreases from 16.7 to $6.1 n_c$ and the FWHM target thickness increases from 18 to 44 μm as τ was increased from 3 to 6 ns. An imaging magnetic spectrometer (IMS) [28] was used to measure the accelerated ion spectrum along the axis of laser propagation. The measured proton spectra as a function of the delay between the ablation and drive laser are shown in Figs. 1(b)–1(e). With the ablation laser off, the proton spectrum is characteristic of the TNSA mechanism and extends to maximum of ~19 MeV [Fig. 1(b)]. With the ablation laser on, the delay was then increased on consecutive shots. For $\tau = 3$ ns [Fig. 1(c)], the cutoff energy decreases to 11 MeV. This is attributed to the increasing rear scale length of the target, which reduces the TNSA field. Interestingly, at $\tau = 4$ ns, Fig. 1(d) shows that two spectrally narrow and distinct peaks appear at ~10 and ~18 MeV, respectively, in contrast to the usual TNSA continuum. This suggests that an additional acceleration mechanism is present and capable of accelerating narrow distributions of protons to energies comparable to the maximum TNSA cutoff energy. Compared to the unablated foil, at $\tau = 4$ ns, the number of escaping electrons was observed to increase 4× [26]. This is consistent with the increased laser coupling and heating required to produce CSA protons. For $\tau = 6$ ns [Fig. 2(e)], no protons > 5 MeV were observed. These results clearly show an optimal acceleration regime at $\tau = 4$ ns, indicating that the production of narrow energy distributions is sensitive to the plasma density profile at this time.

Figure 2 and additional spectra detailed in Supplemental Material [26] show that, at $\tau = 4$ ns, spectra with narrow peaks of protons were consistently observed at energies between 7.9 and 17.7 MeV. At this delay, a narrow distribution of heavier ions with a peak velocity within 30% of the proton peak velocity was also consistently seen. The observation of multiple species of ions with different charge-to-mass ratios being accelerated to similar velocities and into narrow distributions is consistent with the reflection and acceleration from a moving potential associated with a collisionless shock and not expected to result from TNSA. Differential filtering of the IMS image plate detector allowed for discrimination between proton and heavier ion spectral features [26]. Because of having the same Z/A ratio, differentiating between C^{6+} and O^{8+} ions using the IMS or TP was not possible. The ion signal is assumed to be comprised predominantly of C^{6+} ions as the Mylar target has 2.5× more carbon than oxygen ions.

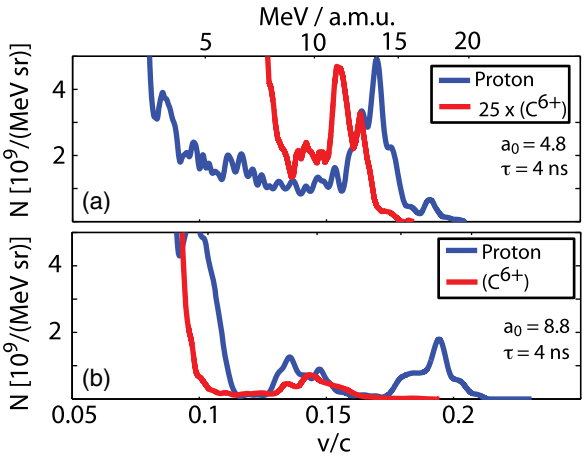

FIG. 2. (a),(b) The observed proton and ion velocity spectrum measured at the optimal delay of $\tau = 4$ ns. In (a) and (b), the drive laser power was held constant while the laser focus was varied, changing the incident a_0 from 4.8 to 8.8, respectively.

While the production of narrow distributions of protons and ions at similar velocities was consistently observed at a $\tau = 4$ ns, the spectral shape and peak energy of these distributions was observed to vary shot to shot and to be sensitive to the incident laser spot size. Shot to shot, the energy and energy spread of the higher-velocity peak was observed to vary between 11.3 and 17.7 MeV and 8.5% and 15.8%, respectively, as the incident a_0 was varied between 8.1 and 8.8. Additionally, as seen in Figs. 2(a) and 2(b), at the same incident laser power, the spectral distribution of protons was observed to change when the spot size was increased and the incident a_0 reduced to 4.8. The variation in energy and spectral shape is thought to arise from differences in laser-plasma coupling and heating. This is influenced by shot-to-shot variations in the laser focusing and resulting intensity due to the thermal lensing of the laser, the plasma density profile, self-focusing, and target alignment. Similar energy variation is common in other high-intensity laser plasma acceleration schemes [29].

Within the FWHM of the proton peaks at 13.5 and 17.7 MeV observed in Figs. 2(a) and 2(b), the total number of protons was estimated to be $3.2 \pm 0.9 \times 10^9$ and $1.0 \pm 0.6 \times 10^9$, respectively. Measurements at these conditions show a proton beam divergence of ~24°. The number of accelerated protons observed is substantially higher (~10^4×) than obtained in previous CSA experiments conducted at lower densities and intensities with 10 μm wavelength lasers. Moreover, the higher-energy, narrow spread, peak shown in Fig. 2(b) contains a similar (~80%) charge to the TNSA beam shown in Fig. 1(b) at the same energy and bandwidth. This shows that CSA can represent a significant advantage for applications requiring narrow energy spread beams, since it would avoid the beam transmission losses and added complexity associated with energy-selection techniques of broadband TNSA beams. Experiments using magnetic-field-based techniques to reduce the bandwidth of TNSA beams have been limited to 0.1% transmission efficiencies [30,31]. Recent simulations of more advanced electro-optics indicate that under optimal conditions the transmission efficiency

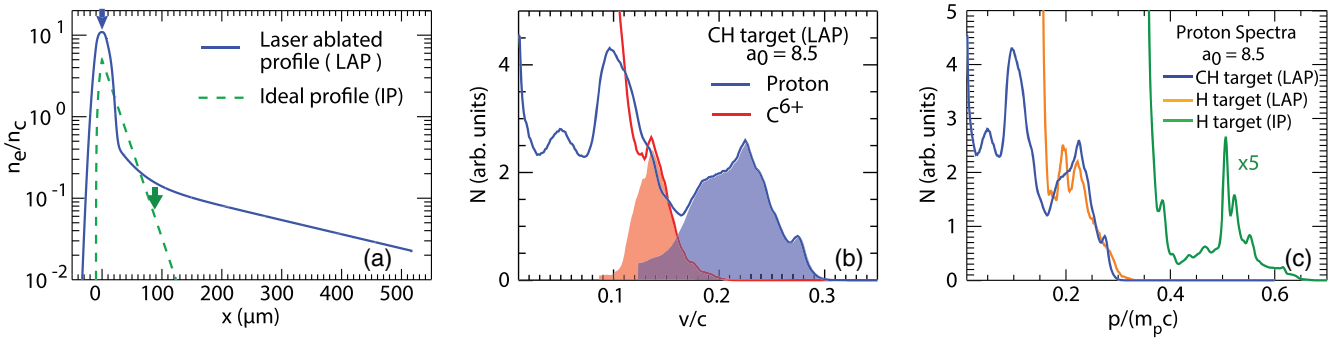

FIG. 3. Ion spectra produced from PIC simulations using different plasma profiles and ion compositions. (a) Initial electron density profile, with the dashed and solid curves denoting the theoretical idealized profile (IP) [21] and the expected laser ablated profile (LAP) of the experiment at $\tau = 4$ ns from HYDRA calculations, respectively. In these simulations, a 1 ps laser with $a_0 = 8.5$ irradiates the target from the left to produce the shock wave. For each profile, the location at which shock reflection begins is denoted by an arrow. (b) The proton and C^{6+} spectrum produced from a CH plasma with a LAP. The shaded region denotes the shock-reflected portion of the spectra as identified from the ion velocity phase space. (c) Comparison of the proton spectra obtained with the same laser for a CH target with a LAP (blue curve), a pure H target with a LAP (orange curve), and a pure H target with an IP (green curve, with the amplitude multiplied by 5).

at 60–200 MeV can approach 5%–20% [32,33]. At energies between 5 and 8 MeV, the transmission through a set of four quadrapoles was inferred to range between ~15% and 100% [34].

IV. SIMULATIONS

In order to better understand how the LAP and multi-ion species plasma impact the scaling of ion acceleration with laser intensity, 2D PIC simulations with OSIRIS 3.0 [35] were performed. The simulations modeled the interaction of the drive laser pulse ($\lambda_0 = 1$ μm, $\tau_0 = 1$ ps, and $a_0 = 8.5$) with a CH plasma for the experimentally expected profile obtained with HYDRA at $\tau = 4$ ns [Fig. 3(a)]. The LAP has a peak density of $n_e = 11 n_c$ and a FWHM of thickness $L = 25$ μm, followed by a long low-density exponential profile with a scale length of $L_g = 250$ μm at the rear side. In order to simulate the temporal dynamics of the interaction, a long and narrow simulation box was used that extended 830 and 10 μm in the direction along and transverse to the laser propagation, respectively [36].

The simulations confirm the formation of an electrostatic shock with $v_s \sim 0.045c$ that reflects both protons and C^{6+} ions from the upstream plasma to $\sim 0.09c$. Shock reflection starts near the peak density of the plasma [blue arrow in Fig. 3(a)] soon after the laser reaches peak intensity. The sharp change in the density profile near $n_e \sim 0.5 n_c$ at the rear side of the plasma (where the ablation laser is absorbed) leads to the generation of a localized space-charge electric field. As shock-reflected protons (C^{6+} ions) experience this field, they gain an additional velocity $v_{\text{sheath}} \sim 0.13c (\sim 0.05c)$. The differences in v_{sheath} are mostly due to the different Z/A ratios of the two species. After this region, the typical TNSA field is strongly suppressed due to the long density scale length, and the maximum velocity remains the same. This leads to a final velocity of the C^{6+} ions within ~35% of the proton velocity, similar to the experiments. Moreover, the final particle spectra obtained are also consistent with the experimental observations, showing peaks with energies (and energy spreads) of 23 MeV ($\Delta E/E = 64\%$) for protons and 9 MeV/amu ($\Delta E/E = 33\%$) for C^{6+} ions [Fig. 3(b)]. The energy spread is mostly determined by the temporal evolution of the shock, which slows down due to dissipation by ion reflection [37]. The (slice) energy spread at each reflection point is significantly smaller: 19% for C^{6+} and 8% for protons.

Simulations conducted with the same laser and electron density profile, but with a pure hydrogen plasma, show that the spectrum of reflected protons is very similar to the case of a CH plasma [Fig. 3(c)]. This indicates that the presence of multiple ion species does not significantly affect the maximum obtainable velocity. However, the presence of multiple ion species is found to change the expansion dynamics downstream of the shock, inducing modulations in the lower-energy portion of the spectrum, as seen in Fig. 3(b) and in some of the experimental results. This will be discussed in more detail elsewhere.

The impact of the experimental LAP on particle acceleration was investigated by comparing these results with those obtained in simulations where the same laser interacts with a hydrogen target with the theoretical ideal profile (IP) discussed in Ref. [21]. The IP has a sharp linear rise over 10 μm on the front side, followed by an exponential profile on the rear side with a scale length $L_g = 20$ μm [Fig. 3(a)]. The FWHM thickness of the target is $L = 17.5$ μm. For a fixed density profile, it was found that a peak density of $n_e = 5 n_c$ maximizes the energy gain by CSA. For these conditions, the laser absorption and electron temperature is higher than with the LAP, as described by Eq. (1). An electrostatic shock is formed with $v_s \sim 0.145c$. At such a high velocity, the shock cannot efficiently reflect the upstream protons initially. In this case, CSA requires the

upstream protons to be first accelerated in the controlled TNSA field, which reduces their kinetic energy in the shock frame. For the density scale length $L_g = 20$ μm, protons acquire $v_{\mathrm{sheath}} \sim 0.22c$, before they are reflected by the shock. The final proton beam energy is $E = 113$ MeV with $\Delta E/E = 4\%$ [Fig. 3(c)], consistent with the CSA energy scaling [21]. While the energy obtained with the IP is significantly higher, the total number of protons contained in the reflected beam is ~30× smaller than in the LAP. This is because efficient reflection begins only at the rear side of the target near $n_e \sim 0.1 n_c$ as seen in Fig. 3(a).

These results indicate that the plasma profile controls both the charge and energy of CSA beams. Laser ablation of thinner foils (< 0.5 μm) may allow the production of plasmas with $n_e \sim 5 n_c$ and $L \sim 17.5$ μm that, with the laser used in these experiments, is estimated to produce ~80 MeV proton beams. Simulations indicate that further tuning of the rear-side density scale length to $L_g \sim 20$ μm would produce proton beams with > 100 MeV but with less charge.

V. CONCLUSIONS

In conclusion, we report on the first experimental evidence of efficient CSA of narrow distributions of protons and heavier ions using a high-intensity 1 μm wavelength laser with a peak $a_0 \sim 8.5$. By tuning the plasma profile using laser ablation, beams with energies up to 18 MeV/amu and energy spreads of 10%–20% containing up to 3×10^9 particles were produced. The number of particles in these distributions was $10^4\times$ higher than previous CSA work conducted with 10 μm wavelength laser systems. These results demonstrate the ability of CSA to efficiently accelerate high yield, narrow distributions of ions to meet the needs of applications. Additionally, the simultaneous acceleration of ion beams with different Z/A ratios to similar velocities offers a promising source for more accurately diagnosing the electromagnetic fields of high-energy-density plasmas. Results from PIC simulations are consistent with the experimental data and reveal that the control of the plasma profile allows the optimization of the beam charge or energy, depending on the application needs. Precise shaping of near-critical density plasma profiles would allow the generation of >100 MeV/amu with the same laser system. This could be achieved in the future by reducing the foil thickness, by changing the wavelength of the photons used to ablate the target (e.g., x rays), or by directly fabricating the profile via 3D printing.

ACKNOWLEDGMENTS

We thank H. Chen and A. Hazi for their support of these experiments and C. Curry, A. Kemp, and C. Roedel for valuable discussions. This work and the use of the Jupiter Laser Facility was performed under the auspices of the U.S. Department of Energy (DOE) under Contract No. DE-AC52-07NA27344, with support from the Lawrence Livermore National Laboratory (LLNL) Laboratory Directed Research and Development Program (15-LW-095). Additional support was provided by U.S. DOE under Contracts No. DE-AC02-76SF00515, No. DE-SC0010064, and No. DE-NA0001944, the DOE Office of Science, Fusion Energy Sciences under field work proposal (FWP) 100237, FWP 100182, FWP 100331, and SCW1575-1, National Nuclear Security Administration (NNSA) Grant No. DE-NA0002950, NSF Grant No. 1734315, and Natural Sciences and Engineering Research Council Grant No. RGPIN-2014-05736. The work at University of California, Los Angeles (UCLA) was supported by NNSA Grant No. DE-NA0003873. The authors acknowledge the OSIRIS Consortium, consisting of UCLA and Instituto Superior Técnico (Portugal) for the use of the OSIRIS 3.0 framework and the visXD framework. Simulations were conducted on Mira (Argonne Leadership Computing Facility) through an ALCC award and on Vulcan (LLNL).

[1] D. Kraus *et al.*, Formation of diamonds in laser-compressed hydrocarbons at planetary interior conditions, Nat. Astron. **1**, 606 (2017).

[2] O. A. Hurricane *et al.*, Inertially confined fusion plasmas dominated by alpha-particle self-heating, Nat. Phys. **12**, 800 (2016).

[3] J. S. Ross *et al.*, Transition from Collisional to Collisionless Regimes in Interpenetrating Plasma Flows on the National Ignition Facility, Phys. Rev. Lett. **118**, 185003 (2017).

[4] E. L. Clark, K. Krushelnick, J. R. Davies, M. Zepf, M. Tatarakis, F. N. Beg, A. Machacek, P. A. Norreys, M. I. K. Santala, I. Watts, and A. E. Dangor, Measurements of Energetic Proton Transport through Magnetized Plasma from Intense Laser Interactions with Solids, Phys. Rev. Lett. **84**, 670 (2000).

[5] P. K. Patel, A. J. Mackinnon, M. H. Key, T. E. Cowan, M. E. Foord, M. Allen, D. F. Price, H. Ruhl, P. T. Springer, and R. Stephens, Isochoric Heating of Solid-Density Matter with an Ultrafast Proton Beam, Phys. Rev. Lett. **91**, 125004 (2003).

[6] G. M. Dyer, A. C. Bernstein, B. I. Cho, J. Osterholz, W. Grigsby, A. Dalton, R. Shepherd, Y. Ping, H. Chen, K. Widmann, and T. Ditmire, Equation-of-State Measurement of Dense Plasmas Heated With Fast Protons, Phys. Rev. Lett. **101**, 015002 (2008).

[7] J. Fernández, B. Albright, F. Beg, M. Foord, B. Hegelich, J. Honrubia, M. Roth, R. Stephens, and L. Yin, Fast ignition with laser-driven proton and ion beams, Nucl. Fusion **54**, 054006 (2014).

[8] P. M. Nilson, L. Willingale, M. C. Kaluza, C. Kamperidis, S. Minardi, M. S. Wei, P. Fernandes, M. Notley, S. Bandyopadhyay, M. Sherlock, R. J. Kingham, M. Tatarakis, Z. Najmudin, W. Rozmus, R. G. Evans, M. G. Haines, A. E. Dangor, and K. Krushelnick, Magnetic Reconnection and Plasma Dynamics in Two-Beam Laser-Solid Interactions, Phys. Rev. Lett. **97**, 255001 (2006).

[9] R. A. Snavely, M. H. Key, S. P. Hatchett, T. E. Cowan, M. Roth, T. W. Phillips, M. A. Stoyer, E. A. Henry, T. C. Sangster, M. S. Singh, S. C. Wilks, A. MacKinnon, A. Offenberger, D. M. Pennington, K. Yasuike, A. B. Langdon, B. F. Lasinski, J. Johnson, M. D. Perry, and E. M. Campbell, Intense High-Energy Proton Beams from Petawatt-Laser Irradiation of Solids, Phys. Rev. Lett. **85**, 2945 (2000).

[10] V. T. Tikhonchuk, A. A. Andreev, S. G. Bochkarev, and V. Y. Bychenkov, Ion acceleration in short-laser-pulse interaction with solid foils, Plasma Phys. Controlled Fusion **47**, B869 (2005).

[11] S. S. Bulanov, A. Brantov, V. Y. Bychenkov, V. Chvykov, G. Kalinchenko, T. Matsuoka, P. Rousseau, S. Reed, V. Yanovsky, D. W. Litzenberg, K. Krushelnick, and A. Maksimchuk, Accelerating monoenergetic protons from ultrathin foils by flat-top laser pulses in the directed-Coulomb-explosion regime, Phys. Rev. E **78**, 026412 (2008).

[12] T. Esirkepov, M. Borghesi, S. V. Bulanov, G. Mourou, and T. Tajima, Highly Efficient Relativistic-Ion Generation in the Laser-Piston Regime, Phys. Rev. Lett. **92**, 175003 (2004).

[13] B. M. Hegelich, B. J. Albright, J. Cobble, K. Flippo, S. Letzring, M. Paffett, H. Ruhl, J. Schreiber, R. K. Schulze, and J. C. Fernández, Laser acceleration of quasi-monoenergetic MeV ion beams, Nature (London) **439**, 441 (2006).

[14] C. A. J. Palmer, N. P. Dover, I. Pogorelsky, M. Babzien, G. I. Dudnikova, M. Ispiriyan, M. N. Polyanskiy, J. Schreiber, P. Shkolnikov, V. Yakimenko, and Z. Najmudin, Monoenergetic Proton Beams Accelerated by a Radiation Pressure Driven Shock, Phys. Rev. Lett. **106**, 014801 (2011).

[15] A. Henig, S. Steinke, M. Schnürer, T. Sokollik, R. Hörlein, D. Kiefer, D. Jung, J. Schreiber, B. M. Hegelich, X. Q. Yan, J. Meyer-ter Vehn, T. Tajima, P. V. Nickles, W. Sandner, and D. Habs, Radiation-Pressure Acceleration of Ion Beams Driven by Circularly Polarized Laser Pulses, Phys. Rev. Lett. **103**, 245003 (2009).

[16] S. Kar, K. F. Kakolee, B. Qiao, A. Macchi, M. Cerchez, D. Doria, M. Geissler, P. McKenna, D. Neely, J. Osterholz, R. Prasad, K. Quinn, B. Ramakrishna, G. Sarri, O. Willi, X. Y. Yuan, M. Zepf, and M. Borghesi, Ion Acceleration in Multispecies Targets Driven by Intense Laser Radiation Pressure, Phys. Rev. Lett. **109**, 185006 (2012).

[17] S. Palaniyappan, C. Huang, D. C. Gautier, C. E. Hamilton, M. A. Santiago, C. Kreuzer, A. B. Sefkow, R. C. Shah, and J. C. Fernández, Efficient quasi-monoenergetic ion beams from laser-driven relativistic plasmas, Nat. Commun. **6**, 10170 (2015).

[18] D. Haberberger, S. Tochitsky, F. Fiuza, C. Gong, R. A. Fonseca, L. O. Silva, W. B. Mori, and C. Joshi, Collisionless shocks in laser-produced plasma generate monoenergetic high-energy proton beams, Nat. Phys. **8**, 95 (2012).

[19] O. Tresca, N. P. Dover, N. Cook, C. Maharjan, M. N. Polyanskiy, Z. Najmudin, P. Shkolnikov, and I. Pogorelsky, Spectral Modification of Shock Accelerated Ions Using a Hydrodynamically Shaped Gas Target, Phys. Rev. Lett. **115**, 094802 (2015).

[20] L. O. Silva, M. Marti, J. R. Davies, R. A. Fonseca, C. Ren, F. S. Tsung, and W. B. Mori, Proton Shock Acceleration in Laser-Plasma Interactions, Phys. Rev. Lett. **92**, 015002 (2004).

[21] F. Fiuza, A. Stockem, E. Boella, R. A. Fonseca, L. O. Silva, D. Haberberger, S. Tochitsky, C. Gong, W. B. Mori, and C. Joshi, Laser-Driven Shock Acceleration of Monoenergetic Ion Beams, Phys. Rev. Lett. **109**, 215001 (2012).

[22] Y. V. Medvedev, Evolution of a density disturbance in a collisionless plasma, Plasma Phys. Controlled Fusion **56**, 025005 (2014).

[23] C. Gong, S. Y. Tochitsky, F. Fiuza, J. J. Pigeon, and C. Joshi, Plasma dynamics near critical density inferred from direct measurements of laser hole boring, Phys. Rev. E **93**, 061202 (2016).

[24] T. Grismayer, P. Mora, J. C. Adam, and A. Héron, Electron kinetic effects in plasma expansion and ion acceleration, Phys. Rev. E **77**, 066407 (2008).

[25] F. Fiuza, A. Stockem, E. Boella, R. A. Fonseca, L. O. Silva, D. Haberberger, S. Tochitsky, W. B. Mori, and C. Joshi, Ion acceleration from laser-driven electrostatic shocks, Phys. Plasmas **20**, 056304 (2013).

[26] See Supplemental Material at http://link.aps.org/supplemental/10.1103/PhysRevAccelBeams.21.103401 for details on the experimental methods and measurements.

[27] M. M. Marinak, G. D. Kerbel, N. A. Gentile, O. Jones, D. Munro, S. Pollaine, T. R. Dittrich, and S. W. Haan, Three-dimensional HYDRA simulations of National Ignition Facility targets, Phys. Plasmas **8**, 2275 (2001).

[28] H. Chen, A. U. Hazi, R. van Maren, S. N. Chen, J. Fuchs, M. Gauthier, S. L. Pape, J. R. Rygg, and R. Shepherd, An imaging proton spectrometer for short-pulse laser plasma experiments, Rev. Sci. Instrum. **81**, 10D314 (2010).

[29] J. Fuchs, P. Antici, E. d'Humières, E. Lefebvre, M. Borghesi, E. Brambrink, C. A. Cecchetti, M. Kaluza, V. Malka, M. Manclossi, S. Meyroneinc, P. Mora, J. Schreiber, T. Toncian, H. Pépin, and P. Audebert, Laser-driven proton scaling laws and new paths towards energy increase, Nat. Phys. **2**, 48 (2006).

[30] T. Toncian, M. Borghesi, J. Fuchs, E. d'Humières, P. Antici, P. Audebert, E. Brambrink, C. A. Cecchetti, A. Pipahl, L. Romagnani, and O. Willi, Ultrafast laser-driven microlens to focus and energy-select mega-electron volt protons, Science **312**, 410 (2006).

[31] M. Schollmeier *et al.*, Controlled Transport and Focusing of Laser-Accelerated Protons with Miniature Magnetic Devices, Phys. Rev. Lett. **101**, 055004 (2008).

[32] F. Schillaci, M. Maggiore, L. And, G. Cirrone, G. Cuttone, F. Romano, V. Scuderi, L. Allegra, A. Amato, G. Gallo, G. Korn, R. Leanza, D. Margarone, G. Milluzzo, and G. Petringa, Design of a large acceptance, high efficiency energy selection system for the ELIMAIA beam-line, J. Instrum. **11**, P08022 (2016).

[33] U. Masood, M. Bussmann, T. E. Cowan, W. Enghardt, L. Karsch, F. Kroll, U. Schramm, and J. Pawelke, A compact solution for ion beam therapy with laser accelerated protons, Appl. Phys. B **117**, 41 (2014).

[34] F. Schillaci, L. Pommarel, F. Romano, G. Cuttone, M. Costa, D. Giove, M. Maggiore, A. Russo, V. Scuderi, V. Malka, B. Vauzour, A. Flacco, and G. Cirrone, Characterization of the ELIMED Permanent Magnets Quadrupole system prototype with laser-driven proton beams, J. Instrum. **11**, T07005 (2016).

[35] R. A. Fonseca, L. O. Silva, F. S. Tsung, V. K. Decyk, W. Lu, C. Ren, W. B. Mori, S. Deng, S. Lee, T. Katsouleas, and J. C. Adam, *Lecture Notes in Computer Science* (Springer, Berlin, 2002), pp. 342–351.

[36] The simulation resolved this domain with 32768×384 cells, used a time step $\Delta t = 0.058$ fs, 16 particles per species per cell, and cubic particle shapes, and ran for ~4 ps. The boundary conditions were open or absorbing in the longitudinal direction and periodic transversely.

[37] A. Macchi, A. S. Nindrayog, and F. Pegoraro, Solitary versus shock wave acceleration in laser-plasma interactions, Phys. Rev. E **85**, 046402 (2012).